RSC Advances

PAPER

Manipulating light emission of quantum dots by simultaneously controlling crystal morphology and doping†

Cite this: *RSC Adv.*, 2014, **4**, 2614

Hsueh-Shih Chen,*[a] Bertrand Lo[b] and Jhen-Yu Huang[b]

Received 11th October 2013
Accepted 25th November 2013

DOI: 10.1039/c3ra45727c

www.rsc.org/advances

This study reports the feasibility of manipulating light emission of spherical and non-spherical ZnSe quantum dots doped with iodine at the crystal surface or matrix. Experimental results suggested that photoluminescence of both spherical and non-spherical ZnSe quantum dots was significantly dependent on the dopant radial position. On the other hand, the crystal morphology was found to affect the doping state of iodine in the quantum dots. The doped iodine of the spherical and non-spherical quantum dots was mainly at the crystal surface and matrix, respectively. The spherical quantum dots doped with iodine exhibited photoluminescence at about 510 nm, while non-spherical ones showed much longer wavelength (~580 nm) and higher emission efficiency. The results reveal a new way to design luminescent materials *via* simultaneously controlling crystal morphology and doping.

Introduction

Since the invention of transistors and the development of semiconductor industries in the middle of the last century, doping, a technique that intentionally introduces impurities into bulk crystals, has been used to manipulate material properties such as the conductivity and light harvesting for semiconductive materials.[1] From the 1990s, control over the dimension of nanostructured materials has drawn much attention from researchers because it provides a feasible way to change material properties by simply varying their size, which is due to so-called the quantum confinement effect (QCE). Semiconductive quantum dot (QD) material, for example, is considered one of the promising nanomaterials for future electronic devices due to its unique size-tunable optical absorption, photoluminescence (PL) and electronic behaviors.[2] Recently, doping of QDs has become attractive to scientists for the study of fundamental theories and the development of new energy materials and devices.[3] Besides the impurity-doping and the size-control techniques, some studies have also demonstrated that by controlling the materials morphology it is possible to adjust the properties of nanomaterials such as photoluminescence and the carrier distribution.[4] So the morphology-tunable ability has shown potential for adjusting and creating novel properties for energy materials.

Bulk ZnSe is a well-known luminescent material with the emission wavelength ~460 nm and the bandgap energy (E_g) ~2.7 eV. Spherical ZnSe QDs have been proved to have size-dependent bandgap energy with monochromatic emission wavelength from 400 to 450 nm.[5] Besides the size effect, we have demonstrated that either crystal morphology[4a] or doping[6] can affect PL properties of ZnSe QDs as well. For example, with internal doping of iodine, electronic band structure of spherical ZnSe QDs displayed extra deep states related to iodine, showing distinct luminescence properties compared with undoped samples. Regarding the morphological effect of ZnSe QDs, it was found that PL from intrinsic non-spherical ZnSe QDs displayed an extraordinarily wide emission band arisen from the carrier recombination in both core-related states and surface-related states, which offered a warm colour with good color rendering for lighting devices.[4a] As either morphology or doping are capable of changing the carrier recombination path of ZnSe QDs, in this paper, we prepare iodine-doped ZnSe QDs with both spherical and tailored crystal morphology, and investigate their photoluminescence with respect to varied morphology, doping and the combination of the two.

Experimental

Syntheses of spherical ZnSe QDs from ZnO were reported previously.[5] In the present study for non-spherical ZnSe QDs, zinc acetate was used as received. Synthesis, doping and ZnS passivation of non-spherical ZnSe were carried out in a one-pot synthesis. Zn precursor was prepared from Zn acetate/hexadecylamine (HDA)/lauric acid (LA) (4 mmol/40 mmol/3.8 mmol) at 150 °C. Internally iodine-doped non-spherical ZnSe QDs were synthesized by the layer-by-layer (LBL) growth method

[a]*Department of Materials Science and Engineering, National Tsing Hua University, Hsinchu 300, Taiwan. E-mail: sean.chen@cantab.net*

[b]*Material and Chemical Laboratories, Industrial Technology Research Institute, Kuan-Fu Road Sec. 2, Hsinchu 300, Taiwan*

† Electronic supplementary information (ESI) available. See DOI: 10.1039/c3ra45727c

This journal is © The Royal Society of Chemistry 2014

similar to that of spherical ZnSe QDs prepared from ZnO.[6] Briefly, several sets of the alternating iodine-monomer (TOP–Se–I) injections and Se-monomer injections (TOP–Se) were used to grow interlaced dopant–host layers on ZnSe cores. TOP–Se–I precursor was prepared by 0.04 mmol iodine, 4 mmol Se and 4 ml TOP. TOP–Se was prepared by dissolving 0.1 mmol Se into 1 ml trioctylphosphine (TOP). ZnSe cores were first produced by injecting 0.2 ml of TOP–Se into hot Zn precursor at 300 °C for couple of minutes depending on a desired size. Then, alternating TOP–Se–I (0.8 ml) and TOP–Se (0.2 ml) injections were performed every 30 s. ZnS shell was grown by injecting S precursor (0.3 mmol S in 1 ml TOP) into the reaction vessel. Samples prepared by LBL-doping are referred to ZnSe:$[I/ZnSe]_n$ QDs (n = number of the I/ZnSe layers). Surface iodine-doped ZnSe QDs were prepared by monomers-mixing method (mix-doping) using a mixture of the TOP–Se–I and TOP–I precursors. The specimens were characterized by X-ray diffractometer (XRD, XD-D1 Shimadzu), high-resolution transmission electron microscope (JEOL JEM-4000EX). Photoluminescence (PL, Hitachi 4500) from samples dried in vacuum was performed at 325 nm excitation wavelength.

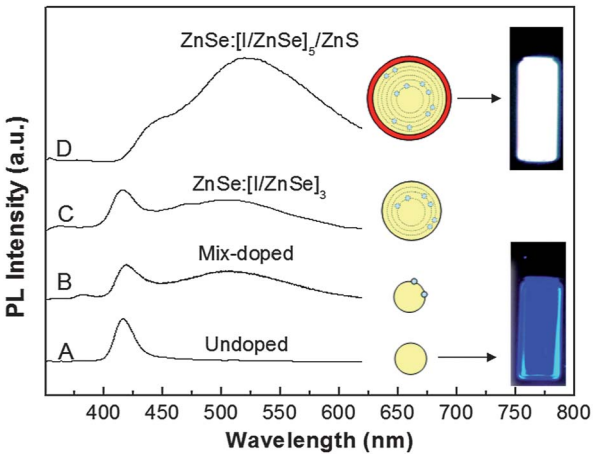

Fig. 1 PL spectra from spherical ZnSe QDs; undoped (curve A), mix-doped (curve B), and doped by layer-by-layer overcoating with three I/ZnSe layers (ZnSe:$[I/ZnSe]_3$) (curve C), and five I/ZnSe layers plus ZnS shell (ZnSe:$[I/ZnSe]_5$/ZnS) (curve D). The inset displayed digital photos of spherical ZnSe QDs and ZnSe:$[I/ZnSe]_5$/ZnS QDs dispersed in toluene under 365 nm UV excitation.

Results and discussion

Doping of spherical ZnSe QDs

Internal doping of semiconductor II–VI QDs was found to be difficult. Although some studies have shown that using specific monomers allows to internally doping II–VI QDs,[7] in most of the cases impurity atoms were predominately bounded on the surface of QDs.[8] This phenomenon has been attributed to the surface-purification of nanocrystals (impurities are automatically expelled from the matrix) or weak binding between dopants or the crystal surface.[3,9,10] Unfortunately, the electronic properties of the surface doped QDs could not be completely manipulated, which can be judged by PL spectra exhibiting both core-related and surface-related carrier recombination. A general method of internally doping QDs has been proposed recently, *i.e.*, *in situ* layer-by-layer (LBL) growth, in which impurity layers and host layers are sequentially grown on QDs cores.[6] In the LBL doping method, impurity atoms are kinetically encapsulated with several additional host layers by a series of impurity and host monomers injections. In that case, either the self-purification mechanism or the mechanism of weak binding energy of the dopant–crystal surface could be negligible in the doping process. Fig. 1 (curve A) shows that PL from intrinsic spherical ZnSe QDs (dia. ~4.5 nm) is monochromatic at 416 nm ($E_g \sim 3.0$ eV), which is larger than that of bulk ZnSe due to the QCE.[11] Surface-doped spherical ZnSe:I QDs prepared by the conventional mixed-monomers (named mix-doping) method displays that both of core-related emission (due to QCE) and impurity-related emission at 512 nm ($E_g \sim 2.4$ eV) are present in the PL spectra (curve B), indicating that surface dopants only partly alter the electronic band structure of ZnSe QDs. For the internally iodine-doped spherical ZnSe:$[I/ZnSe]_n$ QDs from the LBL process, the core-related PL could be completely switched to the impurity-related PL by five [I/ZnSe] layers (curves C and D). The impurity-related PL band is broad (425–700 nm) and peaks at ~ 512 nm, which has been assigned to the deep-level emission associated with the lattice defects caused by the iodine substitution to Se in the ZnSe matrix. However, the emission from the spherical ZnSe:$[I/ZnSe]_n$ QDs have much shorter wavelength compared with that from ZnSe epitaxial film doped by iodine (580–620 nm).[12] Indeed, introduction of iodine atoms into a ZnSe matrix could cause various types of the recombination centers. It is known that the spectral width of the deep-level recombination in iodine-doped ZnSe epitaxy films was related to a strong lattice coupling.[13] Doping of iodine in ZnSe could cause deep impurities-related acceptor levels because of the compensation effect and lattice defects such as Zn vacancies. The defect centers are able to form some complexes and interact with the carriers, which are present in the form of broad band in the 500–700 nm region that is so-called deep-level emission. The emission directly associated with iodine is generally in the longer wavelength range. For instance, iodine-doped ZnSe epitaxial films prepared by vapor phase epitaxy (VPE) displayed a broad emission band at around 580 nm, which was attributed to the self-activated (SA) emission induced by iodine.[12] The lattice defects, however, led to relatively shorter wavelength at around 510–520 nm for ZnSe QDs in the present case.

Non-spherical ZnSe QDs

Previous study has shown that PL from ZnSe QDs was morphologically changed.[4a,5] For shape-tailored non-spherical ZnSe QDs (Fig. 2(a)), they exhibited a ultra-broad PL band (400–700 nm) comprising of a monochromatic blue emission peak arisen from ZnSe core (maximum ~ 425 nm) and a broad band covering green–yellow–red range (maximum ~ 510 nm) (ESI†). In those QDs, the distorted lattices may destroy the symmetry and the periodicity of the crystal structure that perturbs the QDs energy band structure.

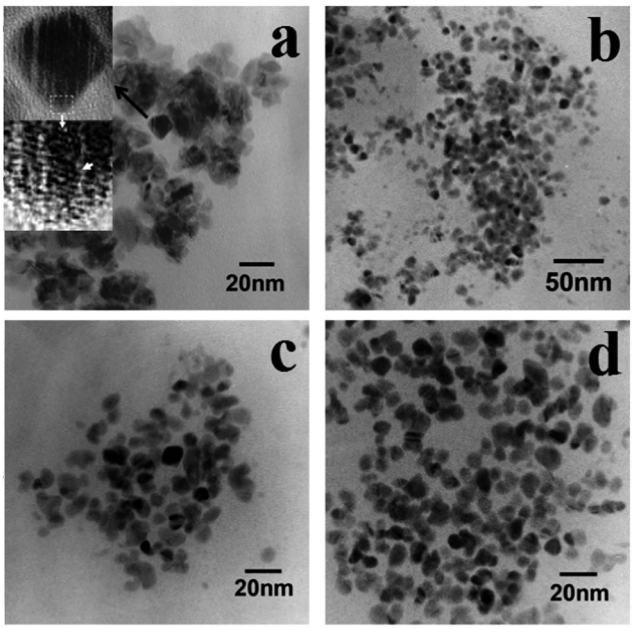

Fig. 2 TEM images of non-spherical ZnSe synthesized from ZnO (a), non-spherical ZnSe synthesized from Zn acetate in low resolution (b) and in high resolution (c), and ZnSe:[I/ZnSe]$_5$/ZnS QDs from Zn acetate (d). The inset in image a displays the distorted lattices.

Thus, extra local energy potentials could exist near the surface and affect the carrier dynamics in ZnSe QDs. This local perturbation effect finally results in a series of the deep energy levels which lie within the band gap and hence a sub-band-gap broad PL could be observed. By comparing the PL spectra of spherical ZnSe:[I/ZnSe]$_5$ QDs with that of intrinsic non-spherical ones, there is a similarity in their deep-level emission bands. Both QDs samples possess a broad band in the 450–650 nm range with the maximum at around 510 nm. Presumably, the lattice defects caused by the iodine substitution in ZnSe QDs and the surface strained lattice of non-spherical ZnSe QDs are similar. Deconvolution of the PL spectra with Gaussian function does show some certain relationship between two QDs samples (ESI†). Both samples show emission bands from the ZnSe cores, the donor–pair pair (DAP) recombination, and the deep energy levels.[14] But it may be argued that the deep-level spectrum might be not in the form of a function (*e.g.* Gaussian distribution) and may have an asymmetric shape, especially in highly doped crystalline semiconductors.[15] If the distributions of the deep-level states of the band diagram in both situations (surface-strained lattice defects or iodine-induced lattice defects) are similar, the carrier transitions would not significantly vary but the density of states would increase when the deep-level states in two situations overlaps with each other. This may be observed in PL spectra if the iodine atoms are introduced to the strained surface lattice of non-spherical ZnSe QDs (will be discussed later). The structural defects induced by either the distorted surface or the doping of the iodine substitution, in any case, play an essential role in the carrier recombination for ZnSe QDs.

Non-spherical ZnSe QDs in the current study were synthesized from Zn acetate, as shown in a TEM image (Fig. 2(b)). The non-spherical ZnSe QDs have similar morphology to those from ZnO (Fig. 2(a)) but show a lower degree of aggregation (Fig. 2(c)). The passivation of ZnS was performed by the last injection of the sulfur precursor, forming ZnSe:[I/ZnSe]$_5$/ZnS QDs, as shown in Fig. 2(d). The non-spherical morphology of the ZnSe QDs did not significantly change when the growth time increased and/or extra monomer injections were introduced into the system. This result suggests that the non-spherical morphology was the result of the equilibrium shape for ZnSe QDs in the synthetic condition.

The non-spherical morphology for ZnSe QDs is believed to be dominated by the surfactants used in the synthesis.[5] Moreover, II–VI wurtzite materials are intrinsically anisotropic and have faster growth rate along the *c*-axis,[16] where metal atoms on the (001) and (00$\bar{1}$) possess one and three dangling bonds, respectively.[17] Taking a well-known example of synthesis of CdSe QDs, the coordinating surfactants such as TOPO or alkyl phosphonic acid can not passivate all three dangling bonds of a single Cd toms of (00$\bar{1}$) that leads to a higher chemical potential and faster reaction rate on this face. So the non-spherical morphology could be reasonably obtained for wurtzite ZnSe QDs.

Fig. 3(a) presents XRD data of intrinsic non-spherical ZnSe (curve A) and iodine-doped non-spherical ZnSe QDs prepared by conventional monomers-mix-doping (curve B) and LBL-doping methods (curves C and D). All samples possess the hexagonal (wurtzite) crystal structure. It has been found that the diffraction peaks broaden for those iodine-doped samples since the substitution of iodine in the Se lattice site (I_{Se}) may decrease the ZnSe crystallinity[18] and/or increase the non-uniform strain of the ZnSe lattice. This may be due to that the I_{Se} ions cause formation of dangling bonds such as –Zn–I or Zn– vacancies. The full width at half maximum (FWHM) of the diffraction peak (inset in Fig. 3(a)) increases up to 22.7% for ZnSe:[I/ZnSe]$_5$ QDs, while there is only a slight change (<1%) for ZnSe:I QDs, consistent with the fact that iodine could be only introduced to the ZnSe surface by the monomers-mix-doping method.[6] Moreover, I^- ion has larger crystal ionic radius (~2.06 Å) than that of Se^{-2} one (~1.84 Å), and the substitution of I to Se is able to increase the I–Zn distance that expands the ZnSe lattice. Besides, it is known that Zn anion might react with iodine to form ZnI_2.[19] So the diffraction peaks would shift to a lower angle for the internally iodine-doped ZnSe QDs. Fig. 3(b) gives the profile fitting of (100), (002), and (101) diffraction peaks and the peak shifts with respect to coating layers (upper inset) in the LBL-doping method. All diffraction peaks shift to lower angles with increasing overcoats of I/ZnSe layer. It is interesting that the face (101) has a relatively large shift compared with the other two. This result implies that the (101) face of the non-spherical ZnSe QDs plays a certain role for the iodine doping. One of the possible explanations is that the reaction between iodine ions and the ZnSe (101) face was more feasible on the non-spherical ZnSe QDs. It was reported that the {101} faces of wurtzite CdSe nanocrystals grow more slowly than the (00$\bar{1}$) ones, which could be eventually replaced by (101) equivalent faces in the crystal growth.[17] In the current study, the (101) facet on the ZnSe cores is thought to be present and provides a higher doping probability for iodine. The inset in Fig. 3(b) schematically shows the lattice images of a wurtzite ZnSe QD. The (101)

 This journal is © The Royal Society of Chemistry 2014

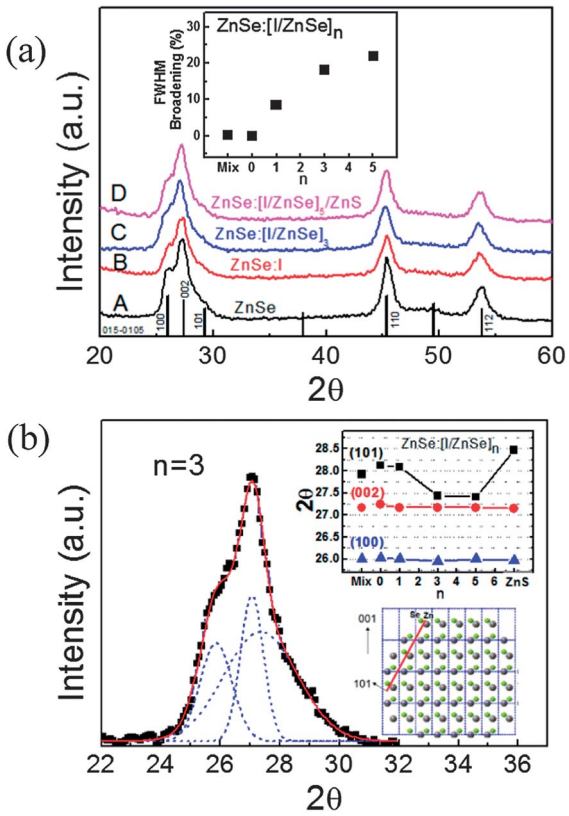

Fig. 3 (a) XRD of non-spherical ZnSe (curve A), ZnSe:I (mix-doping, curve B), ZnSe:[I/ZnSe]$_3$ (LBL-doping, curve C), and ZnSe:[I/ZnSe]$_5$/ZnS QDs (curve D). The inset shows broadening of FWHM of (110) peak of ZnSe:I and ZnSe:[I/ZnSe]$_n$ (n = 1, 3, 5) QDs relative to pure ZnSe QDs. (b) Profile fitting of the diffraction peak of ZnSe:[I/ZnSe]$_3$. The insets show the peak position of the regenerated diffraction peaks (top) and sketch of the lattice image of a wurtzite ZnSe QD (bottom).

face is shown as a red line and red dashed line represents the unit cell. Another possibility is that the reaction between iodine monomers and Se on the (101) is faster than the other faces. The detailed mechanism needs further investigation. In addition, the passivation of ZnS shell slightly shifts the diffraction peak to a larger angle, reflecting the fact that the sulfur possesses smaller ionic radius.

Iodine-doped non-spherical ZnSe QDs

Fig. 4 gives PL spectra from non-spherical ZnSe QDs with and without iodine doping. Intrinsic non-spherical ZnSe QDs display a broad PL band composed of a blue band and a deep-level emission one (curve A) similar to those prepared from ZnO.[4] The DAP emission at around 465 nm shows that the distorted surface lattice could create shallow defect centers within the band diagram of ZnSe QDs, which is similar to the impurities in ZnSe epitaxial films prepared by VPE.[18] PL spectra from non-spherical ZnSe:I QDs synthesized by the monomers-mixing-doping method are quite similar to that from intrinsic non-spherical ZnSe QDs (curve B in Fig. 4) but the PL intensity is significantly enhanced. This result implies that the distribution of the deep-level states is not significantly altered but the

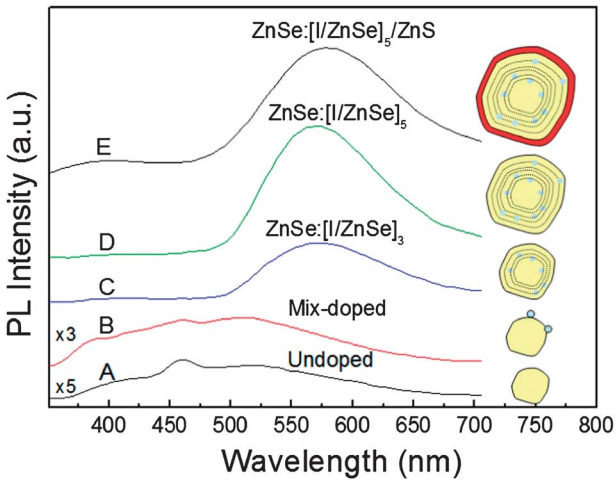

Fig. 4 PL spectra from non-spherical ZnSe QDs undoped (curve A), mix-doped (curve B), and doped by layer-by-layer overcoating with three (curve C) and five I/ZnSe layers (curve D), and five I/ZnSe layers plus ZnS shell (curve E).

density of states is dramatically increased. Since it is known that the iodine predominately situated at the surface of non-spherical ZnSe QDs from the monomers-mix-doping method, the unchanged PL characteristics indicates that the surface-doping of iodine simply produces more energy states in the band diagram for the non-spherical ZnSe QDs, inferring the deep-level emission mechanisms in intrinsic non-spherical ZnSe QDs and iodine-doped spherical ZnSe QDs are similar.

For internally iodine-doped non-spherical ZnSe QDs prepared by the LBL-doping method, doping of iodine completely switched the core-related emission to the longer wavelength range. The emission associated with the lattice defects is (~510 nm) eliminated by the LBL-doping, while that associated with typical SA centers of iodine-doped ZnSe (~580 nm) is enhanced. With three [I/ZnSe] layers, non-spherical ZnSe:[I/ZnSe]$_3$ QDs solely exhibits an yellow-emitting emission band at ~575 nm. This result is similar to the SA emission from iodine-doped ZnSe epitaxial films from VPE. The PL integration intensity of non-spherical ZnSe:[I/ZnSe]$_5$ QDs is about 13 times of that from the intrinsic non-spherical ZnSe QDs. Overcoating with an additional ZnS shell, ZnSe:[I/ZnSe]$_5$/ZnS QDs do not show significant improvement of PL intensity but emission wavelength slightly red shifts to 582 nm.

Photoluminescence mechanism

Fig. 5 presents the band diagram of spherical and non-spherical ZnSe QDs in different doping conditions according to the PL spectra. Intrinsic spherical ZnSe QDs displays a single sharp PL peak with larger band gap energy (E_g ~ 3.0 eV) from ZnSe cores due to the QCE. PL from surface iodine-doped spherical ZnSe QDs shows both core-related (E_g ~ 3.0 eV) and deep-level emissions (E_g ~ 2.4 eV). The internally iodine-doped spherical ZnSe QDs possess only a broad deep-level emission band, which is dominated by the lattice defects induced by iodine doping. PL from intrinsic non-spherical ZnSe QDs also exhibits both

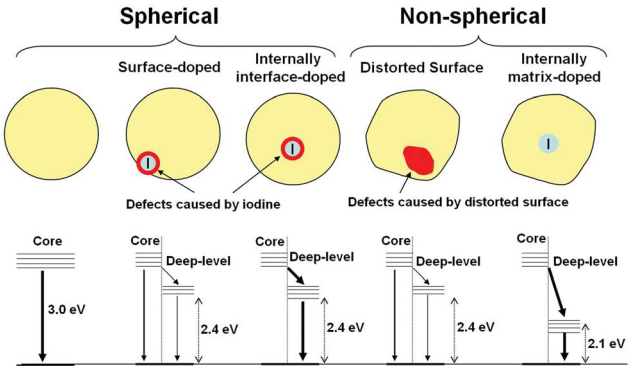

Fig. 5 PL mechanism of ZnSe QDs in different doping conditions.

core-related ($E_g \sim 3.0$ eV) and deep-level emissions ($E_g \sim 2.4$ eV), which resembles that from surface iodine-doped spherical sample. For the internally iodine-doped non-spherical ZnSe QDs, peak position of the deep-level band redshifts ~0.3 eV ($E_g \sim 2.1$ eV) and the emission wavelength changes from green (~510 nm) to yellow (~580 nm) range.

The non-spherical ZnSe QDs are found to be more dopable. Compared with spherical ZnSe:$[I/ZnSe]_5$ QDs, most of the carrier recombinations in non-spherical ZnSe:$[I/ZnSe]_5$ QDs are directed to the typical SA emission at ~580 nm directly associated with iodine as that observed in iodine-doped ZnSe epitaxial films. Also, the emission efficiency of non-spherical ZnSe:$[I/ZnSe]_5$ QDs was found to be much higher than either spherical ZnSe:$[I/ZnSe]_5$ or intrinsic non-spherical ZnSe QDs and approached to that of a commercial YAG:Ce phosphor (quantum yield ~45%). The improved PL efficiency is assigned to the suppression of the nonradiative recombination. For spherical ZnSe cores having relatively smooth surface, integration of iodine atoms into ZnSe matrix is relatively difficult because less structural defects such as steps or kinks are present on the crystal surface.[20] On the other hand, the distorted surface lattice of non-spherical ZnSe QDs provides more high energy sites for monomer adsorption so the integration of iodine monomers on the ZnSe cores would be more feasible, and thus formation of defects in the growth process could be suppressed. Another possible reason is that the spherical ZnSe QDs were obtained by interrupting the growth of growing crystals, where the (101) face is not dominant in the kinetic regime, so doping of iodine becomes more difficult.

Considering the effect of iodine doping on PL efficiency for non-spherical QDs, it increases with number of the coating layers (3.2%, 5.5%, 6.5%, 22.9%, 40.3% for bare ZnSe, mix-doped ZnSe:I, ZnSe:[I/ZnSe], ZnSe:$[I/ZnSe]_3$ and ZnSe:$[I/ZnSe]_5$, respectively). The enhanced PL intensity could be related to passivation or elimination of nonradiative centers in the QD matrix by introduced iodine atoms and I/ZnSe coatings. As the luminescence properties of ZnSe QDs are strongly dependent on the defects (*e.g.* Zn vacancies), incorporated iodine ions might replace the nonradiative centers and possibly interact with Zn anions to form some complexes. So additional radiative centers could be created and thus the PL was intensified. Further studies will be focused on mechanism and effect of the doping level on PL properties.

Conclusions

Internal and surface iodine doping of ZnSe QDs in both spherical and non-spherical shapes have been investigated in this study. By varying the shape and the doping of ZnSe QDs, various carrier recombination paths and photoluminescence of ZnSe QDs have been demonstrated. It has been found that the crystal morphology can affect the doping state and photoluminescence of ZnSe QDs. For spherical ZnSe QDs, iodine doping produced photoluminescence at ~512 nm ($E_g \sim 2.4$ eV) relating to the lattice defects, which is similar to intrinsic ZnSe QDs having distorted lattice. For non-spherical ZnSe QDs, the doping produces distinct photoluminescence results ($\lambda_{em} \sim 580$ nm, $E_g \sim 2.1$ eV). This study has shown that distinct carrier dynamics and photoluminescence may be achieved by combining doping and varied morphology of ZnSe QDs, which is beneficial to develop high efficient luminescent materials.

Acknowledgements

This work was supported by the National Science Council of Taiwan under Contract no. NSC 102-2218-E-007-013-MY3 and Industrial Technology Research Institute.

Notes and references

1 (*a*) K. Yokota, K. Nakamura, T. Ishizu, M. Sakaguchi, H. Takano and M. Kumagai, *J. Appl. Phys.*, 1999, **86**, 6697; (*b*) R. N. Bhargava and D. Gallapher, *Phys. Rev. Lett.*, 1994, **72**, 416; (*c*) T. Takeuchi, Y. Harada, T. Tokushima, M. Taguchi, Y. Takata, A. Chainani, J. J. Kim, H. Makino, T. Yao, T. Yamamoto, T. Tsukamoto, S. Shin and K. Kobayashi, *Phys. Rev. B: Condens. Matter Mater. Phys.*, 2004, **70**, 245323; (*d*) N. P. Armitage, F. Ronning, D. H. Lu, C. Kim, A. Damascelli, K. M. Shen, D. L. Feng, H. Eisaki, Z. X. Shen, P. K. Mang, N. Kaneko, M. Greven, Y. Onose, Y. Taguchi and Y. Tokura, *Phys. Rev. Lett.*, 2002, **88**, 257001.

2 (*a*) H. Mattoussi, L. H. Radzilowski, B. O. Dabbousi, E. L. Thomas, M. G. Bawendi and M. F. Rubner, *J. Appl. Phys.*, 1998, **83**, 7965; (*b*) H. S. Chen, C. K. Hsu and H. Y. Hong, *IEEE Photonics Technol. Lett.*, 2006, **18**, 193–195; (*c*) M. D. Goodman, J. Xu, J. Wang and Z. Lin, *Chem. Mater.*, 2009, **21**, 934; (*d*) H. S. Chen and R. V. Kumar, *J. Mater. Chem.*, 2011, **21**, 5928; (*e*) H. S. Chen, M. Ando and N. Murase, *Mater. Lett.*, 2011, **65**, 3146.

3 (*a*) S. C. Erwin, L. Zu, M. I. Haftel, A. L. Efros, T. A. Kennedy and D. J. Norris, *Nature*, 2005, **436**, 91; (*b*) R. Beaulac, P. I. Archer, J. Rijssel, A. Meijerink and D. R. Gamelin, *Nano Lett.*, 2008, **8**, 2949; (*c*) C. Tuinenga, J. Jasinski, T. Iwamoto and V. Chikan, *ACS Nano*, 2008, **2**, 1411; (*d*) M. J. Bowers II, J. R. McBride and S. J. Rosenthal, *J. Am. Chem. Soc.*, 2005, **127**, 15378; (*e*) N. Pradhan, D. M. Battaglia, Y. Liu and X. Peng, *Nano Lett.*, 2007, **7**, 312; (*f*) N. Pradhan, D. Goorskey, J. Thessing and X. Peng, *J. Am. Chem. Soc.*, 2005, **127**, 17586; (*g*) D. Mocatta, G. Cohen, J. Schattner, O. Millo, E. Rabani and U. Banin, *Science*, 2011, **332**, 77.

 This journal is © The Royal Society of Chemistry 2014

4 (*a*) H. S. Chen, S. J. J. Wang, C. J. Lo and J. Y. Chi, *Appl. Phys. Lett.*, 2005, **86**, 131905; (*b*) A. A. Lutich, C. Mauser, E. D. Como, J. Huang, A. Vaneski, D. V. Talapin, A. L. Rogach and J. Feldmann, *Nano Lett.*, 2010, **10**, 4646; (*c*) C. L. Choi, H. Li, A. C. K. Olson, P. K. Jain, S. Sivasankar and A. P. Alivisatos, *Nano Lett.*, 2011, **11**, 2358; (*d*) H. S. Chen and R. V. Kumar, *J. Nanopart. Res.*, 2012, **14**, 1207; (*e*) H. S. Chen and R. V. Kumar, *RSC Adv.*, 2012, **2**, 11586.

5 H. S. Chen, B. Lo, J. Y. Hwang, G. Y. Chang, C. M. Chen, S. J. Tasi and S. J. J. Wang, *J. Phys. Chem. B*, 2004, **108**, 17119.

6 H. S. Chen, H. Y. Horng and R. V. Kumar, *Appl. Phys. Lett.*, 2009, **94**, 141107.

7 D. J. Norris, N. Yao, F. T. Charnock and T. A. Kennedy, *Nano Lett.*, 2001, **1**, 3.

8 P. V. Radovanovic and D. R. Gamelin, *J. Am. Chem. Soc.*, 2001, **123**, 12207.

9 G. M. Dalpian and J. R. Chelikowsky, *Phys. Rev. Lett.*, 2006, **96**, 226802.

10 D. J. Norris, A. L. Efros and S. C. Erwin, *Science*, 2008, **319**, 1776.

11 T. Takagahara and K. Takeda, *Phys. Rev. B: Condens. Matter Mater. Phys.*, 1992, **46**, 15578.

12 (*a*) S. Fujiwara, Y. Namikawa, T. Nakamura and M. Tatsumi, *J. Cryst. Growth*, 2005, **275**, e415; (*b*) T. Muranoi, S. Onizawa and M. Sasaki, *J. Cryst. Growth*, 1994, **138**, 255; (*c*) N. Shibata, A. Ohki and A. Katsui, *J. Cryst. Growth*, 1988, **93**, 703; (*d*) N. Shibata, A. Ohki and S. Zembutsu, *Jpn. J. Appl. Phys.*, 1988, **27**, L251.

13 J. S. Massa, G. S. Buller, A. C. Walker, J. Simpson, K. A. Prior and B. C. Cavenett, *Appl. Phys. Lett.*, 1995, **67**, 61.

14 A. E. Thomas, G. J. Russell and J. Woods, *J. Phys. C: Solid State Phys.*, 1984, **17**, 6219.

15 B. A. Batovski and C. M. Hardalov, *J. Appl. Phys.*, 1993, **74**, 291.

16 X. Peng, L. Manna, W. Yang, J. Wickham, E. Scher, A. Kadavanich and A. P. Alivisatos, *Nature*, 2000, **404**, 56.

17 (*a*) L. Manna, E. C. Scher and A. P. Alivisatos, *J. Am. Chem. Soc.*, 2000, **122**, 12700; (*b*) L. Manna, E. C. Scher and A. P. Alivisatos, *J. Cluster Sci.*, 2002, **13**, 521.

18 T. Muranoi, S. Onizawa and M. Sasaki, *J. Cryst. Growth*, 1994, **138**, 255.

19 O. S. Kumar, S. Soundeswaran and R. Dhanasekaran, *Cryst. Growth Des.*, 2002, **2**, 585.

20 (*a*) H. S. Chen and R. V. Kumar, *J. Phys. Chem. C*, 2009, **113**, 31; (*b*) H. S. Chen and R. V. Kumar, *J. Phys. Chem. C*, 2009, **113**, 12236; (*c*) H. S. Chen and R. V. Kumar, *Cryst. Growth Des.*, 2009, **9**, 4235.

This journal is © The Royal Society of Chemistry 2014